Applied Catalysis A, General 709 (2026) 120664

Contents lists available at ScienceDirect

Applied Catalysis A, General

journal homepage: www.elsevier.com/locate/apcata

Investigation of the ammonia cracking kinetics over Ru/Al_2O_3 using conductive reactor internals

Federico Sascha Franchi, Matteo Ambrosetti, Nicola Usberti, Alessandra Beretta, Gianpiero Groppi, Enrico Tronconi *

Politecnico di Milano, Dipartimento di Energia, Via La Masa 34, Milano 20156, Italy

ARTICLE INFO

Keywords:
Ammonia decomposition
Ru catalyst
Reactor design
Conductive reactor internals
Hydrogen vectors
Heat transfer

ABSTRACT

NH_3 cracking is receiving growing attention for the exploitation of ammonia as H_2 carrier. Of the different aspects of this process that require in depth study, the choice of the optimal catalyst is arguably one of the most important, being the process kinetically controlled. Literature agrees that ruthenium is the most active metal for low temperature ammonia cracking, however, no consensus on the kinetic expression has been reached due to the high sensitivity of the reaction mechanism to the specific reaction conditions. For this reason, it is of utmost importance to work in conditions as close as possible to the industrial ones to derive a reaction rate useful for practical reactor design. This is challenging due to the strong endothermicity of the reaction that leads to non-uniform temperature profiles in concentrated kinetic tests, and the impact of temperature gradients in kinetic studies is well known in the literature. In this study, the activity of a commercial Ru/Al_2O_3 catalyst in the form of small spherical particles was investigated by feeding pure ammonia in the 2500–20'000 $Ncc/h/g_{cat}$ range at up to 3 bar-a as well as by cofeeding reaction products. Despite working with undiluted catalyst and pure ammonia in an integral reactor up to ≅ 100 % NH_3 conversions, the inclusion of a thermally conductive aluminium POCS reactor internal enabled to achieve almost isothermal conditions, resulting in a LHHW rate expression able to fit the whole experimental data set with a MPE less than 5 %.

1. Introduction

In a time when global warming is becoming a paramount problem for mankind, widespread investments and technological shifts are mandatory toward a more sustainable future to mitigate the effects of climate change [1]. Arguably, of the many anthropogenic greenhouse gasses (GHG), the biggest contributor to global warming is CO_2 whose emissions come mainly from the use of fossil fuels [2,3]. In this context, a transition to the so called "hydrogen economy" [4] is one of the best options to drastically reduce the CO_2 emissions. While H_2 as an energy carrier is highly desirable, the technological challenges related to its production, storage and transportation need to be addressed to promote its widespread use. In recent years policies and technological advancement have made production of carbon neutral hydrogen more economically viable; nevertheless, more significant challenges need to be addressed. Blue H_2 (produced from fossil fuels with integrated Carbon Capture, Utilization and Storage, CCUS) and Green H_2 (produced by water electrolysis via renewable energy) are the most promising forms of carbon neutral hydrogen. However, the former has been demonstrated to be technologically feasible but economically viable only at the large scale and the other needs to cope with the intermittent nature of green electricity. Both technologies are, thus, highly dependent on the development of an efficient storage and transportation system for their successful implementation.

Hydrogen has a very high gravimetric energy density at 142 MJ/kg but, due to its extremely low volumetric density (40 kg/m^3 @ 20 °C and 700 bar, gaseous form or 71 kg/m^3 @ -253 °C, liquid), efficient energy storage and transportation of this molecule is highly challenging [5]. One possible solution is the use of the so called "hydrogen carriers", molecules in which H_2 is chemically bound, effectively increasing its density. Among possible alternative carriers, one of the most promising is ammonia. With a global production of more than 150 Mton/year [6], NH_3 is a commodity with a well-established production and handling infrastructure, being the main product in the fertilizers industry. In addition, being NH_3 a liquid at moderate temperatures and pressures (8.5 bar @ 20 °C or -33.3 °C @ 1 bar), it has both very high gravimetric

* Corresponding author.
E-mail address: enrico.tronconi@polimi.it (E. Tronconi).

https://doi.org/10.1016/j.apcata.2025.120664
Received 1 July 2025; Received in revised form 30 September 2025; Accepted 27 October 2025
Available online 28 October 2025

(17.8 %) and volumetric (121 kg_{H_2}/m^3) hydrogen content [7,8]. Nevertheless, to use this molecule as an efficient hydrogen carrier, significant advancements need to be done on its conversion back to H_2.

NH_3 decomposition is a significantly endothermic reaction ($NH_3 \rightarrow {}^3/_2\ H_2 + {}^1/_2\ N_2$, $\Delta H°r = 45.9\ kJ/mol_{NH_3}$) limited by thermodynamic equilibrium [9]. This reaction has been studied since the start of 1900 [10] as the reverse reaction of the NH_3 synthesis and several catalytically active materials have been identified [11]. To this day, the most widely available catalysts on the market are generally based on ruthenium or nickel: they differ mainly because of the temperature range of use, the former being active below 550 °C while the latter is operated at up to 950 °C [12]. Despite the higher price of Ru, the higher activity at low temperature is a key characteristic when a process based on this catalyst needs to fulfil the requirements of compactness, energy efficiency and H_2 purity, e.g. for direct use of H_2 in PEM fuel cells.

Over both materials, the reaction is believed to proceed as a sequence of dehydrogenation steps starting from adsorbed ammonia and ending with the desorption of N_2 and H_2. According to literature, no consensus on the actual RDSs and MASIs has been found, although some common features are well known, like e.g. the poisoning effect of H_2 on Ru. Most of the published works on ammonia cracking propose one of the dehydrogenation steps (typically the second H* extraction) and/or the recombinative desorption of N_2 as the most likely RDS [13–17], with no clear evidence in one direction or the other possibly due to the kinetic relevance of both reactions; as a consequence, rate measurements are highly specific not only to the catalyst under study but also to the investigated experimental conditions (i.e. composition, temperature, pressure [12]), and several reviews provide a very broad picture of best performances so far reported in the literature.

Very few studies have addressed systematic kinetic investigations with the aim of developing kinetic expressions useful for reactor design, with most of the works done on small quantities (50–200 mg) of catalyst powders [14,16] and/or with diluted NH_3 feeds [16]. At this scope, however, the kinetic study must be performed in conditions as close to the industrial operation as possible. Industrial units are expected to operate with pure ammonia, aiming at high conversion; as such, useful kinetic expressions should be able to describe the catalyst activity at high temperature and in a wide range of gas compositions, namely with ammonia concentrations from 100 % down to few percent with a corresponding stoichiometric increase in H_2 and N_2, as well as faithfully predict the effect of space velocity, whose investigation can provide very important information on the evolution of the kinetic dependences with the extent of reaction and guidelines for reactor design [13].

Due to the high endothermicity of the NH_3 decomposition, however, working at high conversion rates implies a significant heat request from the reaction with the risk of developing non negligible thermal gradients across the catalyst bed: of course, accentuated temperature profiles result in additional errors in the evaluation of the intrinsic reaction rate and should be limited as much as possible. In experimental test rigs, the small dimensions of the catalyst bed generally result in low length to diameter ratios and, therefore, in a low flow velocity to operate at high conversions; this results in slow heat transfer rates (mainly controlled by convective phenomena in the packed bed), resulting in non-negligible axial and radial thermal gradients and, in turn, in significant errors in the evaluation of the catalyst activity. Similar difficulties in the management of temperature profiles have already been encountered in the intensification of highly endo/exothermic processes such as steam methane reforming [18,19] and Fischer-Tropsch synthesis [20]. In these instances, the inclusion of highly thermally conductive structured internals proved to be a solution that significantly increased the static heat transfer in the catalyst bed [21–23], reducing the temperature gradients and allowing for more flexibility in the reactor design. In particular, work done in our group demonstrated that the dilution of the catalytic bed with highly thermally conductive granular materials does not provide a significant reduction of thermal gradient when heat loads are sufficiently high due to the discontinuity of the conductive pathway [22], while the inclusion of a continuous conductive matrix such as a periodic open cell structure (POCS) made of a thermally conductive material (e.g. copper or aluminium) is able to significantly flatten the temperature profile [18] by substantially increasing the static conductive heat transfer; moreover, the addition of an external skin to such structures is able to further improve the heat transfer by reducing the wall heat transfer resistance, with a reduction of the radial temperature difference as reported in a recent study of the Fischer-Tropsch synthesis [24]. In the present work, the concept of packed POCS with skin was, thus, implemented to operate the catalytic bed as an isothermal system while investigating the ammonia cracking reaction on a commercial catalyst under industrially relevant conditions (i.e. pure ammonia feed) and exploring the full range of ammonia conversions. The experimental data were then used to derive rate equations in the form both of a power law and of LHHW expressions: such rate equations can be directly applied to the simulation and design of industrial ammonia cracking units.

2. Materials and methods

2.1. Experimental setup

- Commercial catalyst

The ammonia cracking catalyst used in the present work is a commercial product purchased from Heraeus (catalogue name: KT Al2O3 Ru Type K-04502); it consists of egg-shell 2 $\%_{w/w}$ Ru/γ-Al_2O_3 spheres (Fig. 1) with a nominal diameter of 1 mm, i.e. small enough to ensure adequate packing of the catalyst in the POCS cavities. Table 1 summarizes the properties of the catalyst: the average diameter was measured with an optical microscope (SteREO Discovery.V12 equipped with Axiocam ERc 5 s camera, by Zeiss) on a sample of 100 pellets, the Ru content was measured via ICP-MS, the B.E.T. surface area with a Micromeritics TriStar 3000, the pore volume with Micromeritics AutoPore IV mercury porosimeter and CO chemisorption was performed with a ThermoFischer TPD/R/O 1100 as described in [13].

Due to the eggshell nature of the catalyst (as shown in Fig. 1), the local concentration of Ru is significantly higher than the 2 % bulk figure measured via ICP and can be estimated at 7 ± 1 % w/w locally; this high value justifies the very low Ru dispersion found on the fresh catalyst.

Furthermore, the XRD pattern of the catalyst is provided in the SI, Section 1.1.

- 3D printed POCS

In order to limit the temperature gradients in the test reactor, the catalyst spheres were packed in a highly thermally conductive aluminium alloy (AlSi10Mg, [25]) POCS with diamond unit cell [18].

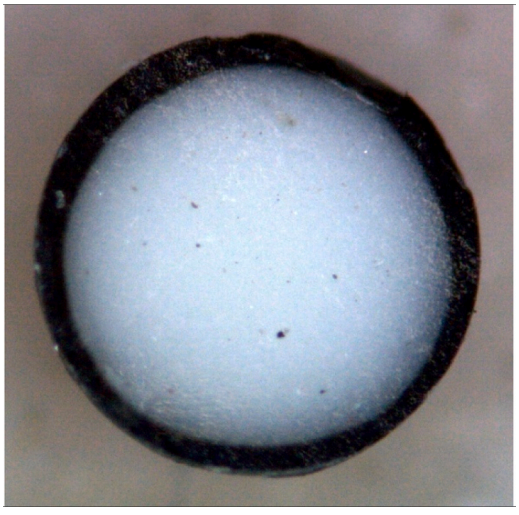

Fig. 1. Optical microscope images of a cross section of the catalyst spheres.

Table 1
Properties of the catalyst spheres.

Diameter [mm]	B.E.T [m^2/g]	Pore volume [ml/g]	Ru content [% w/w]	CO_{uptake}/Ru [mol/mol]
0.954 ± 0.017	152	0.47	1.97 ± 0.05	0.05

The 3D printing of the structure was outsourced to an external company (Aidro Hydraulics) and manufactured via selective laser melting (SLM) followed by lathe machining of the outer surface (Fig. 2). To ensure adequate packing of the catalyst in the open cell structure while keeping a sufficient solid fraction and number of unit cells along the radial reactor coordinate, a cell diameter of 3.5 mm and a strut diameter of 525 μm were selected (Table 2) resulting in a ratio of the window opening to the particle diameter $d_w/d_p = 2.3$ and confirming the possibility to pack successfully the structure [22].

To provide optimal contact and consequently heat transfer between the POCS and the reactor tube (inner diameter = 12 mm), an outer skin of 0.5 mm in thickness was added to the lattice. After 3D printing, the structure was machined, resulting in an external diameter of 11.95 ± 0.05 mm. Moreover, to enable the measurement of the axial temperature profile, a 2 mm hole was opened along the centreline. To ensure easy packing and linearity of the structure, the POCS length was limited to 38.5 mm (11 cells).

- Test reactor design

Reactive tests were performed in a stainless-steel tubular reactor (SS316, ID = 12 mm), assembled as sketched in Fig. 3. Two POCS were inserted in series to enable loading of a sufficient mass of catalyst; great attention was paid to avoiding gaps between the two open cell structures and to preserving the periodicity of the geometry by rotating the elements appropriately; a FeCrAlloy felt disk was placed at the bottom of the catalytic bed to retain the catalyst particles and the stack was placed over a counter tube to ensure proper positioning in the reactor. To allow for the recording of the temperature profiles, a thermowell (external diameter = 2 mm) was inserted along the centreline hole of the stack; a second thermowell was welded to the outside of the reactor tube to measure the corresponding temperature profile on the external reactor wall, as represented in Fig. 3. Two sliding K-type thermocouples were inserted in the thermowells.

The reactor was installed in an electrically heated oven and connected to a dedicated line which enables pure anhydrous ammonia feed. Furthermore, H_2 (purity 4.5), N_2 (purity 5.0) and Ar (purity 5.0) could be fed to the rig from dedicated gas cylinders. The feed gas stream could be fed through the reactor and the catalytic bed as well as through a bypass line, to allow for the analysis of the inlet gas composition. The flow rate of each gas stream was controlled by dedicated mass flow controllers (Brooks Instruments), and the stream composition was analysed with an online mass spectrometer (Hiden Analytical, HPR-20 R&D, QGAsoft software package). To track the total flowrate and improve the quality of the measurements, the streams coming from the reactor and the bypass lines were mixed with additional Ar at a known flowrate to act as a reference gas. Finally, the rig was equipped with a manual back-pressure regulator placed downstream from the reactor: this enabled to run kinetic tests at a pressure of up to 3 bar-a.

2.2. Test procedure

Before running the catalytic tests, possible gas phase NH_3 decomposition activity as well as unexpected reactivity of the stainless-steel tubular reactor and Al POCS were checked by performing blank tests under pure ammonia feed with a gas flow of 500 Ncc/min. Two different runs were performed with and without the POCS inserted (in the latter case filling the reactor with Al_2O_3 spheres in a packed-bed configuration).

After loading the POCS with the catalyst spheres, an in-situ pretreatment was performed feeding 1 % H_2 in Ar at a gas hourly space velocity (GHSV) of 20'000 Ncc/h/g_{cat} and increasing the temperature from room T to 450 °C at 5 °C/min. At the end of the temperature ramp, the catalyst was kept at 450 °C for 1.5 h and cooled to room temperature under a constant stream of Ar. In addition to the packed POCS tests, the catalyst was tested also in a packed bed configuration: the same mass of catalyst (in order to work at the same flowrate) was diluted with inert alumina spheres of the same diameter to obtain the same catalyst bed length as the packed POCS configuration; results are shown in the Supplementary information, Section 2.

2.2.1. Temperature profiles

To verify the ability of the aluminium POCS to limit the development of thermal gradients in the catalyst bed, temperature profiles were measured while performing reactive tests feeding 100 % NH_3 at a GHSV between 2500 and 20'000 Ncc/h/g_{cat} and with oven temperatures in the 440–510 °C range. To perform the measurements, two K-type thermocouples were inserted in the thermowell along the centreline and the reactor wall to the same axial position: when steady-state conditions were reached (for both temperature and concentrations), the measurements from both thermocouples were recorded and the probes moved to the successive coordinate. Temperature measurements were collected every 5 mm starting 7.5 mm upstream from the packed POCS stack and ending 12.5 mm downstream of it. Moreover, to assess the effect of the inclusion of the thermally conductive structure, the same reactive tests were replicated in a conventional packed bed configuration. This configuration was prepared by packing the reactor tube with the same mass of catalyst mixed with inert Al_2O_3 spheres to maintain the minimal dilution provided by the two aluminium POCS.

2.2.2. Kinetic tests

To gather information on the catalyst activity, steady-state tests were performed by feeding 100 % NH_3 at a GHSV between 2500 and 20'000 Ncc/h/g_{cat} and at oven temperatures in the 350–510 °C range with the

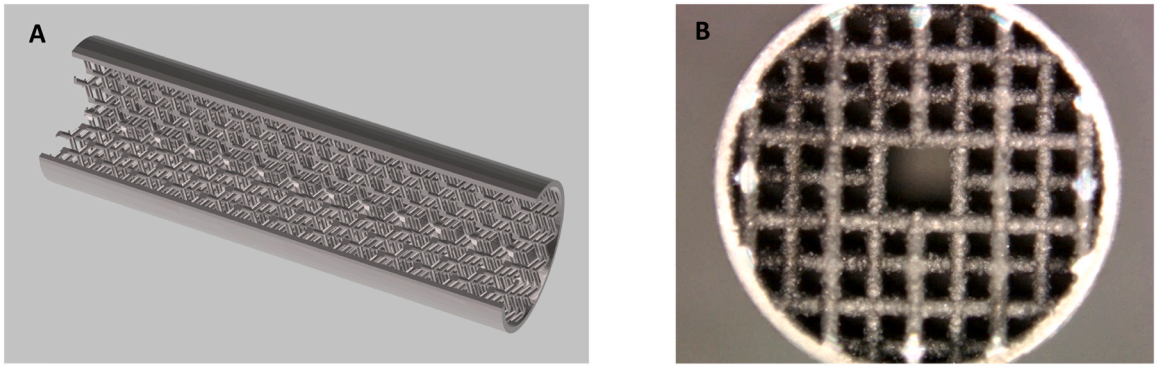

Fig. 2. A) 3D printed AlSi10Mg POCS; B) POCS cross section.

Table 2
Geometrical characteristics of the POCS.

Cell shape	Cell diameter [mm]	Strut diameter [μm]	Void fraction [-]	Specific surface area [m^{-1}]	Internal diameter [mm]	Thermocouple well diameter [mm]	Length [mm]
Diamond	3.5	525	0.894	742	11	2	38.5

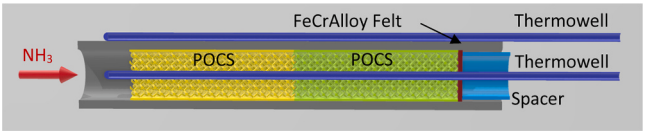

Fig. 3. Longitudinal section of the Dual POCS test reactor.

packed POCS reactor configuration. Moreover, the effect of the operating pressure was investigated by running experiments with pure ammonia feed and setting the overpressure with a backpressure regulator located downstream from the reactor; as reported in literature [14], kinetic studies at moderately low pressure can be extrapolated to the high pressure operating region with minimal deviations, thus the maximum operating pressure was limited to 3 bar. Finally, H_2, N_2 and Ar were co-fed at several molar fractions to investigate the kinetic dependences of the NH_3 decomposition reaction on the concentration of reactant and products. The whole set of experimental conditions is reported in Table 3.

Operating conditions (temperature) were kept stationary for at least 30 min to measure the steady-state activity of the catalyst; then, the oven temperature was step-changed to the next point. Typically, 30 min were enough to ensure a stable ammonia conversion. For all tests, H_2 and N_2 mass balances were checked to ensure a reliable measure (error at steady state condition < 5 %).

2.3. Reactor model and statistical regression analysis

To simulate the kinetic runs, the system was modelled as an integral reactor, assuming ideal plug-flow behaviour under isobaric and isothermal conditions (the validity of the latter assumption will be discussed in Section 3.1.1).

$$\frac{dF_i}{dWcat} = \lambda_i \quad R_{DEC} \tag{1}$$

Where F_i are respectively the ammonia, hydrogen, nitrogen and argon molar flows [mol/s], Wcat is the catalyst load [gcat], λ_i are the stoichiometric coefficients and R_{DEC} is the ammonia decomposition rate $[mol/s/g_{CAT}]$.

Table 3
Plan of experiments.

GHSV [Ncc/h/gcat]	Y_{NH3} [%]	Y_{H2} [%]	Y_{N2} [%]	Y_{Ar} [%]	P [bar]
GHSV effect					
2500	100	0	0	0	1.01
5000	100	0	0	0	1.01
10,000	100	0	0	0	1.01
20,000	100	0	0	0	1.01
Pressure effect					
10,000	100	0	0	0	2.02
10,000	100	0	0	0	3.03
Ar co-feed					
10,000	50	0	0	0	1.01
N_2 co-feed					
10,000	50	0	50	50	1.01
H_2 co-feed					
10,000	75	25	0	0	1.01
10,000	50	50	0	0	1.01
10,000	25	75	0	0	1.01

As input values, the model requires: catalyst load [g_{cat}], GHSV [Ncc/s/g_{cat}], temperature [°C], NH_3, H_2 and N_2 inlet concentrations [ppm] and pressure [bar-a] as independent variables, as well as the experimental conversion of ammonia [$X_{NH3TEST}$, dimensionless].

The differential system constituted by the mass balance equations was integrated numerically and the kinetic parameters were estimated by nonlinear regression minimizing the sum of the squared residuals (F value) [26,27].

$$F = \sum_1^{NTEST} (X_{NH3TEST} - X_{NH3MODEL})^2 \Big/ \sigma^2 \tag{2}$$

Where $X_{NH3TEST}$ and $X_{NH3MODEL}$ are, respectively, the experimental and the simulated ammonia conversions for each experimental condition and σ^2 the variance of the experimental measurements. The overall experimental error variance was estimated as:

$$\sigma^2 = \frac{\sum_{j=1}^{m} \sigma_j^2}{m} \tag{3}$$

where m is the number of experimental temperatures and σ_j^2 was calculated according to:

$$\sigma_j^2 = \frac{\sum_{i=1}^{n} (\chi_{i,j} - \overline{\chi}_j)^2}{n-1} \tag{4}$$

where n is the number of experimental points at each temperature, $\chi_{i,j}$ is the NH_3 conversion for each point i at a given temperature j, and $\overline{\chi}_j$ is the average conversion at temperature j.

3. Results and discussion

Prior to any reactive test, the absence of unwanted catalytic activity from the reactor tube and aluminium POCS was verified: no significant NH_3 conversion was detected (χ_{NH_3} < 1 % @ 500 °C). Based on these data, we ruled out gas-phase reactions and unwanted POCS reactivity, which ensures a correct evaluation of the intrinsic catalyst activity during the experimental campaign.

After installing the two aluminium structures, the Ru/Al_2O_3 spheres were accurately packed reaching a total catalyst inventory of 3.967 g, which results in NH_3 flowrates between 165 Ncc/min (2500 Ncc/h/g_{cat}) and 1320 Ncc/min (20'000 Ncc/h/g_{cat}).

3.1. Kinetic tests

3.1.1. Effects of the operating variables

- Effect of the space velocity

To verify the activity of the catalyst, the effect of GHSV was studied by feeding 100 % NH_3 from 2500 Ncc/h/g_{cat} up to 20'000 Ncc/h/g_{cat}. As already mentioned, given the strong and complex kinetic limitations of the reaction, the effect of space velocity is expected to provide key information for kinetic modelling. The experiments were performed within the temperature range 340–510 °C.

Very limited conversion was observed for temperatures below 350 °C with a maximum conversion of 12 % at 350 °C and 2500 Ncc/h/g_{cat}. Conversion increased sharply with temperature reaching 48.3 % at 400 °C and 2500 Ncc/h/g_{cat} and almost complete conversion at the highest investigated temperature of 510 °C; higher temperatures were avoided to prevent Ru sintering or surface reconstruction phenomena. These tests show a catalyst with a limited sensitivity of the conversion to

the increase of contact time. At a temperature of 450 °C and a GHSV of 20'000 Ncc/h/g_{cat} the maximum measured conversion approached 60 % while a conversion in excess of 95 % was only reached with an eight-fold reduction of the space velocity, down to 2500 Ncc/h/g_{cat}, where the measured conversion approached 100 % only by raising the temperature up to 510 °C. Thermodynamic limitations were not approached in the experimental campaign except at the lowest GHSV of 2500 Ncc/h/g_{cat} and highest temperature of 510 °C with an experimental conversion $\chi_{exp@501°C}$ = 99.58 % vs. $\chi_{eq@501°C}$ = 99.74 % (as shown in Fig. 4).

GHSV = 10'000 Ncc/h/g_{cat} was chosen as the reference space velocity test (NH_3 conversion between 5.7 % @ 354 °C and 89.6 % @ 481 °C) to investigate the effects of reactant and products concentrations and of pressure. Moreover, reproducibility runs were performed at this GHSV (at beginning, mid and end of the experimental campaign) to periodically check the activity of the catalyst (Fig. 5): no significant deactivation of the catalyst was observed after 97 h of operation between the first and the last reproducibility run (of which 42.5 h at T > 450 °C), proving the stability of the catalyst during the whole kinetic investigation.

In addition, the characterization analysis described in Section 2.1, Table 1 was repeated on the spent catalyst highlighting no changes in the support morphology and Ru dispersion (B.E.T. surface area = 148 m^2/g, pore volume = 0.46 ml/g, CO_{uptake}/Ru = 0.05 [mol/mol]).

- *Thermal profiles*

While running the kinetic tests with pure ammonia feed, temperature profiles were collected at the centreline and at the reactor wall to verify the thermal behaviour of the system. Fig. 6 shows the axial temperature profile along the centreline of the reactor (full squares, left y-axis) and the temperature difference between centreline and wall temperature profiles (dotted lines, right y-axis). Indeed, in all the explored conditions, axial gradients were very limited; with increasing space velocity (i.e., at increasing flow rate) the temperature inside the reactor was progressively lower than the oven temperature and only at the highest space velocity it moderately increased along the axial coordinate, mainly due to the significantly lower inlet temperatures. Concerning the radial gradient from the outlet wall to the centreline, it slightly grows with the increasing thermal load of the reaction (i.e., both at increasing temperature, thus conversion, and at increasing flow rate), but even in the worst case it was always within 20 °C and at the reference space velocity of 10,000 Ncc/h/g_{cat} always within 15 °C.

The capability of the reactor configuration in controlling the temperature gradients can be better appreciated by comparing the static

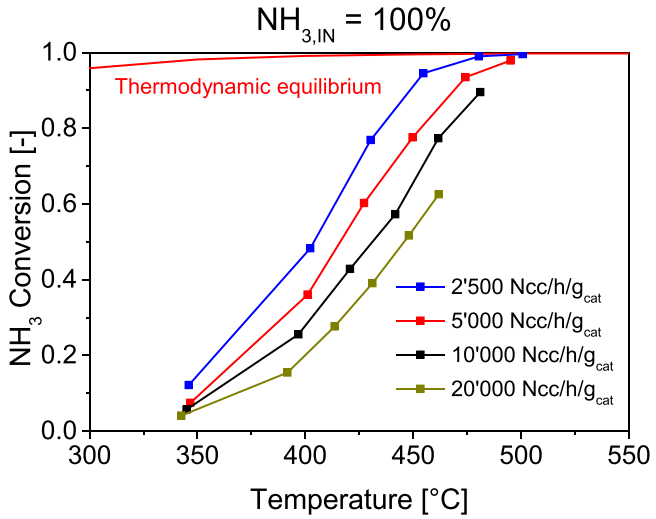

Fig. 4. GHSV effect: NH_3 feed concentration = 100 %, P = 1 bar-a, GHSV from 2500 to 20'000 Ncc/h/g_{gat}.

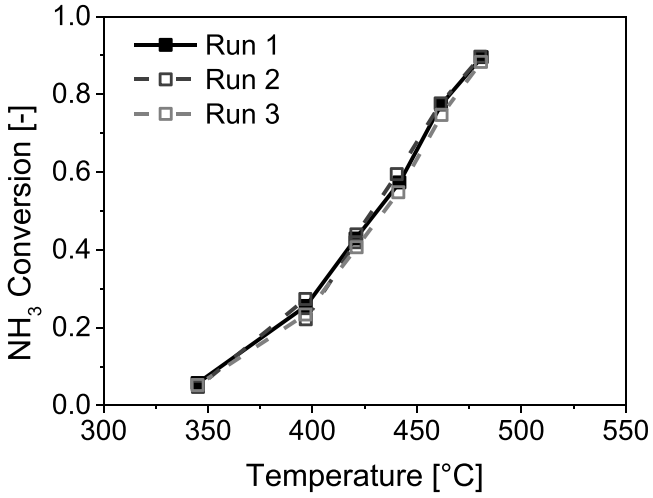

Fig. 5. Reproducibility runs: NH_3 feed = 100 %, P = 1 bar-a, GHSV 10'000 Ncc/h/g_{gat}.

effective thermal conductivity of the POCS structure (47 W/m/K calculated as per Bracconi et al. [21]) against the effective thermal conductivity of a conventional packed bed (0.26 W/m/K calculated as per Specchia et al. [28]). Moreover, a direct experimental comparison of the performances of the two configurations is reported in the SI, Section 2.2.

In view of the almost flat temperature profiles in the packed POCS reactor, a single point measurement of the temperature at approximately 2/3 of the catalyst bed (axial coordinate = 52 mm) was deemed representative of the whole catalyst. This temperature was used for all the following comparisons as well as for the statistical regression analysis (Section 2.3) in which the bed was assumed to be isothermal.

- *Effect of pressure*

The effect of pressure on the catalyst activity was tested between ambient pressure and 3 bar-a. NH_3 conversion results are shown in Fig. 7.

A significant inhibiting effect of pressure was observed; by increasing the absolute operating pressure from 1 bar to 3 bar, a large reduction in conversion occurred in the whole temperature range with a decrease from 77.4 % to 61.4 % at 465 °C and from 89.6 % to 76.0 % at 480 °C. In line with extensive reports in the literature [29], this trend indicates an overall negative kinetic reaction order.

- *Effect of H_2 and N_2 cofeed*

To better assess the kinetic dependencies of the reaction on the different products, tests were runs cofeeding 50 % Ar, 50 % H_2 or 50 % N_2 with NH_3 at the reference GHSV.

As shown in Fig. 8, a reduction of the NH_3 partial pressure in the feed stream by inert dilution (50 % Ar cofeed) resulted in a significant increase of the reaction rate/ammonia conversion as expected from the tests at high pressure in Fig. 7.

By adding 50 % N_2 to the NH_3 feed, no significant difference in the ammonia conversion was detected against the test with Ar cofeed, suggesting no kinetic dependence on the nitrogen partial pressure for this reaction. In stark contrast, a dramatic reduction in the ammonia cracking reaction rate was observed during the hydrogen cofeed tests: NH_3 conversion decreased from 68.4 % (@425 °C, 50 % Ar) to 33.0 % (@430 °C, 50 % H_2).

- *Effect of H_2 cofeed concentration*

To further investigate the kinetic dependence of the reaction rate on the hydrogen partial pressure, tests were performed cofeeding 25 %, 50 % and 75 % hydrogen with ammonia: results are shown in Fig. 9.

Cofeeding H_2 up to 75 % of the total inlet composition resulted in a significant conversion decrease with a more pronounced effect in the low to mid temperature region, indicating a strong negative order in H_2

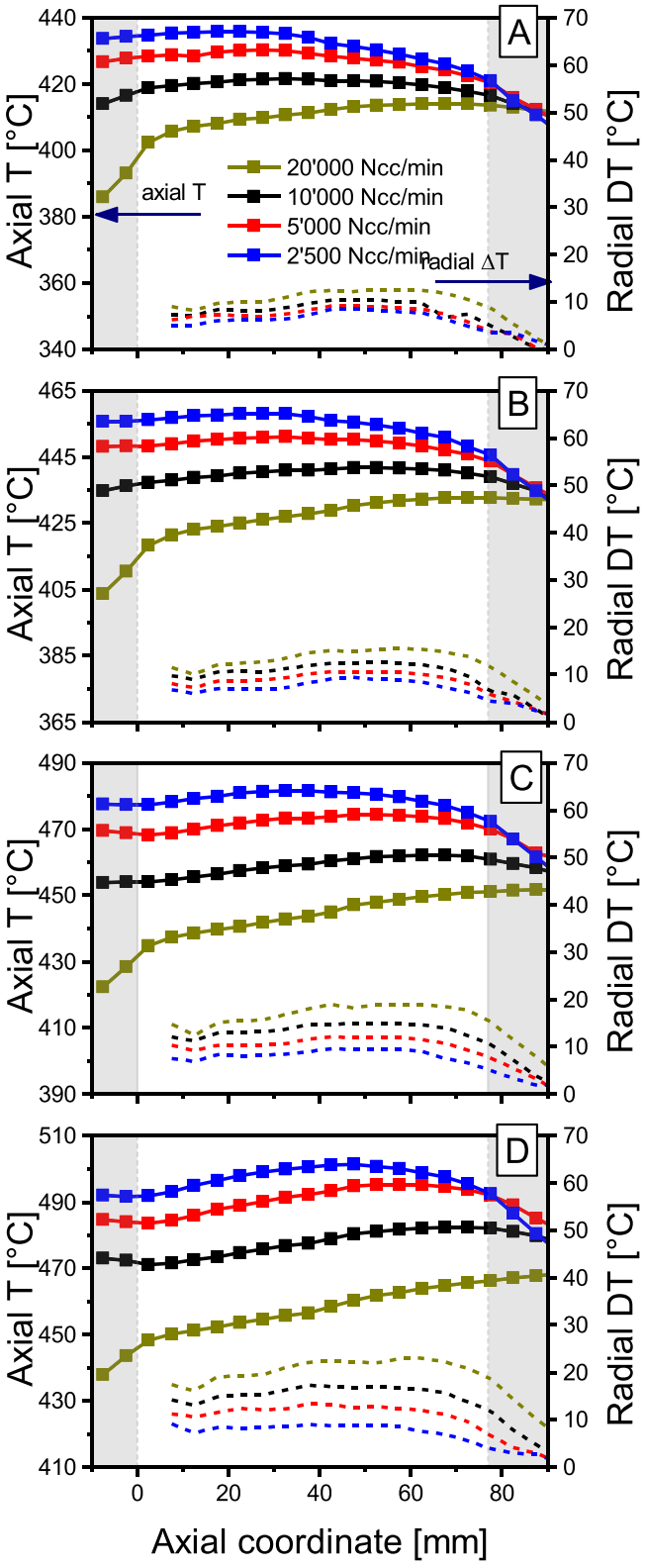

Fig. 6. Axial temperature profiles (symbols) and radial thermal gradients (dashed lines) measured at increasing space velocity and oven temperature in packed POCS.

for the reaction kinetics, i.e., suggesting a strong adsorption of H_2 on the catalyst sites, while at conversions higher than 80 % the inhibiting effect of H_2 cofeed was masked by the large fraction of H_2 produced by the reaction. The latter effect is more clearly seen by comparing the test with

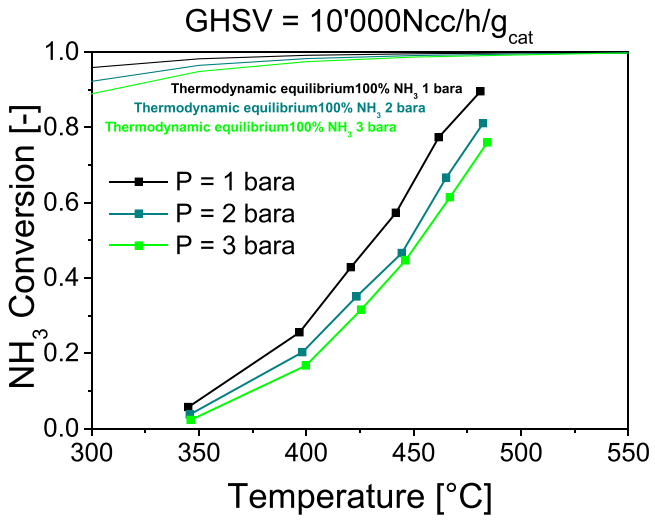

Fig. 7. Pressure effect: NH_3 feed concentration = 100 %, GHSV = 10'000 Ncc/h/g_{gat}, P from 1 to 3 bar-a.

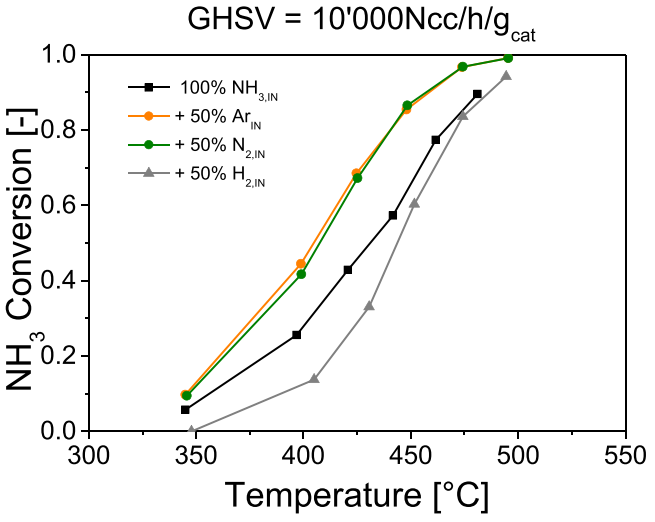

Fig. 8. Effect of products cofeed: GHSV = 10'000 Ncc/h/g_{gat}, P = 1 bar-a, NH_3 = 50 % in N_2 vs H_2 vs Ar.

50 % H_2 and an analogous test with 50 % NH_3 in Ar as shown in Fig. 8. By isolating the inhibition from the dilution effect, it is evident that the negative kinetic order in H_2 is significant across the whole temperature range.

3.2. Kinetic analysis and statistical regression

From the replicated data presented in Fig. 5, a variance of 2.71E-4 was calculated as per Eqs. (3)–(4) and this value was used for all the following statistical analysis.

3.2.1. Empirical power law rate expression

To estimate the global reaction orders of ammonia and hydrogen, an empirical 4 parameter power-law rate expression was adopted:

$$R_{NH3DEC.} = k_{DEC} \quad P^{\alpha}_{NH_3} \quad P^{\beta}_{H_2}(1-\gamma) \tag{5}$$

where α and β are the kinetic orders of ammonia and hydrogen respectively (zero order was assumed for N_2 in accordance with the results reported in Section 3.1.1) and k_{DEC} is the rate constant in the modified Arrhenius form calculated as:

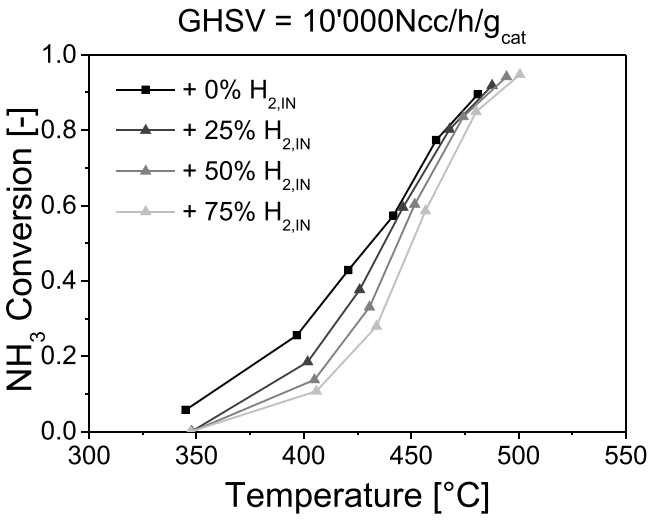

Fig. 9. Effect of H_2 cofeed: GHSV = 10'000 Ncc/h/g_{gat}, P = 1 bar-a, H_2 concentration from 0 % to 75 %.

$$k_{DEC} = k^0_{DEC,T_{ref}} \exp\left(-\frac{E_{ACT}}{R}\left(\frac{1}{T}-\frac{1}{T_{ref}}\right)\right) \quad (6)$$

where T_{ref} = 723.15 K is a temperature in the middle of the experimental range, R the ideal gas constant, $k^0_{DEC,T_{ref}}$ the pre-exponential factor and E_{ACT} the activation energy.

Moreover, being ammonia cracking a reversible reaction, chemical equilibrium was taken into account [14,30–32] with the inclusion of the γ parameter.

$$\gamma = \frac{1}{K_{eq\ therm}} \frac{{P_{H_2}}^{3/2}\ {P_{N_2}}^{1/2}}{P_{NH3}} \quad (7)$$

Where γ incorporates the equilibrium constant $K_{eq\ therm}$ of the ammonia synthesis reaction calculated as described by Sayas et al. [14]. Furthermore, to avoid numerical errors at the reactor inlet (where $P_{H_2,in}$ = 0), the initial partial pressure of H_2 was set to a very small value ($P_{H_2,in}$ = 1E-7).

The full set of data (66 experimental points) collected at different temperature, space velocity, pressure and feed composition, was used to estimate the four rate parameters. These fitted parameters with 95 % confidence limits, the sum of square errors (F, Eq. (2)), the average percentual error (MPE) and the correlation matrix are listed in the following tables (Tables 4, 5 and 6):

Notice the narrow confidence limits of the rate parameter estimates. We ascribe them to the numerosity of the experimental points, to the catalyst stability during the experimental campaign, and specifically to our experimental methodology that ensures negligible thermal gradients along the catalyst bed, resulting in a minimal statistical correlation between the parameter estimates, as also evidenced by Table 5.

This power-law kinetic analysis highlights an exponent slightly less than one in the NH_3 partial pressure and, most importantly, a substantially negative exponent (-1.58) in the partial pressure of H_2, as already reported in previous studies on unpromoted ruthenium-based catalysts (-1.9 Ru/CaO [14]) and significantly lower than what reported for promoted catalysts (-1.2 Ru-K/CaO [14] and -0.42 to -0.54 on Ru-Li/Al_2O_3 [30]); these results well represent the inhibition effect of pressure displayed in Fig. 7. An apparent activation energy of about 46 kcal/mole was estimated, in line with what already proposed in literature [13].

A visualization of the accuracy of this model is provided by the graphical comparison between the experimental data points and the model fit (A–D) and parity plot (E) of Fig. 10, where results of the numerical fit are plotted against the full set of data obtained from the experimental tests.

Table 4
Parameter fit – estimates of the 4 parameters power law, 95 % confidence limit.

	Fit
lnk^0_{DEC}	− 10.16 ± 0.06
E_{ACT} [kcal/mol]	45.82 ± 1.99
α	0.781 ± 0.0434
β	− 1.58 ± 0.096

Table 5
Correlation matrix – 4 parameters power law.

	lnk^0_{DEC}	E_{ACT}	α	β
lnk^0_{DEC}	-	− 0.09	0.50	0.36
E_{ACT}	− 0.09	-	0.62	− 0.84
α	0.50	0.62	-	− 0.53
β	0.36	− 0.84	− 0.53	-

Table 6
Statistical analysis – 4 parameters power law.

F	4.19E-02
MPE	12.32 %
R^2	0.9985

3.2.2. LHHW rate expression

While a simple power law can capture the general behaviour of this catalyst, appreciable deviations are noted at the extremes of the conversion range; a more detailed approach is needed to describe the experimental results with higher accuracy, thus, a LHHW rate expression was identified and used to describe the conversion data.

The following sequence of elementary steps was introduced, as conventionally done in the literature [17,33]:

$NH_3 + s^* \leftrightarrow NH_3^*$ *R1* Adsorption of ammonia
$NH_3^* + s^* \leftrightarrow NH_2^* + H^*$ *R2* First dehydrogenation
$NH_2^* + s^* \leftrightarrow NH^* + H^*$ *R3* Second dehydrogenation
$NH^* + s^* \leftrightarrow N^* + H^*$ *R4* Third dehydrogenation
$2N^* \leftrightarrow N_2 + 2s^*$ *R5* N* desorbs as N_2
$2H^* \leftrightarrow H_2 + 2s^*$ *R6* H* desorbs as H_2

According to the LHHW formalism, different RDS and MARIs were assumed, and the corresponding rate expressions were derived. To discriminate between the possible equations, four criteria resulting from the power law fit were applied:

A. The limited detrimental effect of the pressure implies a slightly negative global kinetic order.
B. Nitrogen has no effect on the catalyst activity, so the final rate expression should not depend on it.
C. The kinetic order of hydrogen must remain negative to account for the significant inhibition of hydrogen observed.
D. Ammonia should have a global kinetic order close to unity.

The kinetic expressions that satisfied all the A–D criteria, were, then, fitted to the experimental data. Further details are reported in the Supplementary information, Section 3.

Of the 20 different rate expressions developed and tested, the best fits of the experimental data were obtained assuming one of the dehydrogenation steps as the rate determining step, in accordance with the results of kinetic studies on a similar unpromoted catalyst (Ru/γ-Al_2O_3) already reported in literature [17] as well as on Ru/CaO [15]. In particular, our data were best described by the following rate equation,

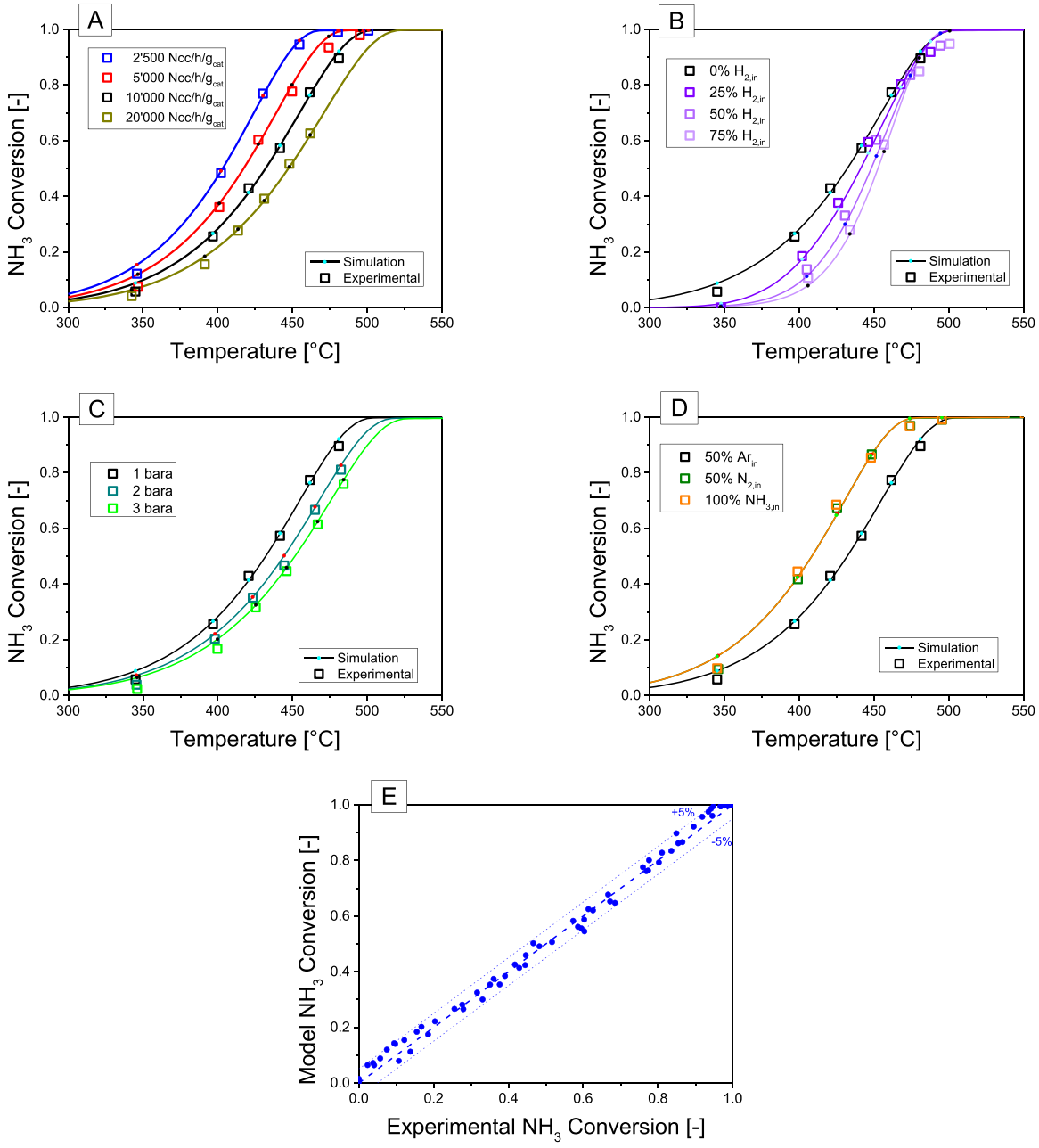

Fig. 10. Experimental versus simulated NH_3 conversion data −4 parameter power law, Eq. (5).

derived under the assumption that the RDS is the second dehydrogenation step (R3) and the MARIs are H^* and NH_3^*:

$$R_{NH3DEC.} = k_{DEC}\frac{P_{NH_3}}{\sqrt{P_{H_2}} \bullet \left(\sqrt{P_{H_2}} + K'_{NH_3^*}P_{NH_3}\right)^2}(1-\gamma) \quad (8)$$

where k_{DEC} is defined according to Eq. (6) while $K'_{NH_3^*}$ is assumed to be T-independent.

The parameter estimates with 95 % confidence limits, the sum of squared errors (F), the average percentual error (MPE) and the correlation matrix are listed in Tables 7, 8 and 9:

As clearly shown by the parity plot (Fig. 11 E) and the statistical analysis results (Table 9), the fitted LHHW rate expression was able to accurately describe the activity of the catalyst in a wide range of experimental conditions. By fitting three kinetic parameters without significant correlations, the model nicely predicts the effects of temperature, pressure, space velocity and reactant/ products concentration

Table 7
Parameter estimates – 3 parameters simplified LHHW RDS 3, NH_3^* and H^* as MARI.

	Fit
lnk^0_{DEC}	− 9.54 ± 0.05
E_{ACT} [kcal/mol]	41.80 ± 1.08
$K'_{NH_3^*}$	0.310 ± 0.045

from very low concentrations to almost complete ammonia conversion. From the MPE, it is also evident that this LHHW model, Eq. (8), provides a better quality of the fit than the simple power law model, Eq. (5). Again, the narrow 95 % confidence limits in Table 7 confirm the accurate estimation of the rate parameters.

The derived kinetic equation indicates the occurrence of a high

Table 8
Correlation matrix – 3 parameters simplified LHHW RDS 3, NH_3^* and H^* as MARI.

	lnk^0_{DEC}	E_{ACT}	$K'_{NH_3^*}$
lnk^0_{DEC}	-	− 0.362	0.862
E_{ACT}	− 0.362	-	− 0.533
$K'_{NH_3^*}$	0.862	− 0.533	-

Table 9
Statistical analysis – 3 parameters simplified LHHW RDS 3, NH_3^* and H^* as MARI.

F	2.12E-02
MPE	5.81 %
R^2	0.9995

surface coverage in all the investigated pressure, temperature and composition domain, switching from adsorbed NH^*_3 when the gas phase concentration of ammonia is high and that of competing H_2 is low (i.e. at low conversion) to adsorbed H* as the MARI on increasing NH_3 conversion or when cofeeding H_2. The ability of the proposed kinetic model to cover an NH_3 conversion range from 1.5 % to 99.7 % makes it promising for the design of different reactor configurations, including NH_3 catalytic crackers for H_2 production as well as partial NH_3 converters for production of H_2 enriched mixtures for low emissions NH_3 burners.

4. Conclusions

The goal of this work was to investigate the kinetics of the ammonia decomposition reaction over a commercial Ru-based catalyst in industrially relevant (concentrated) conditions, in view of developing a rate expression directly applicable to the design of industrial reactors.

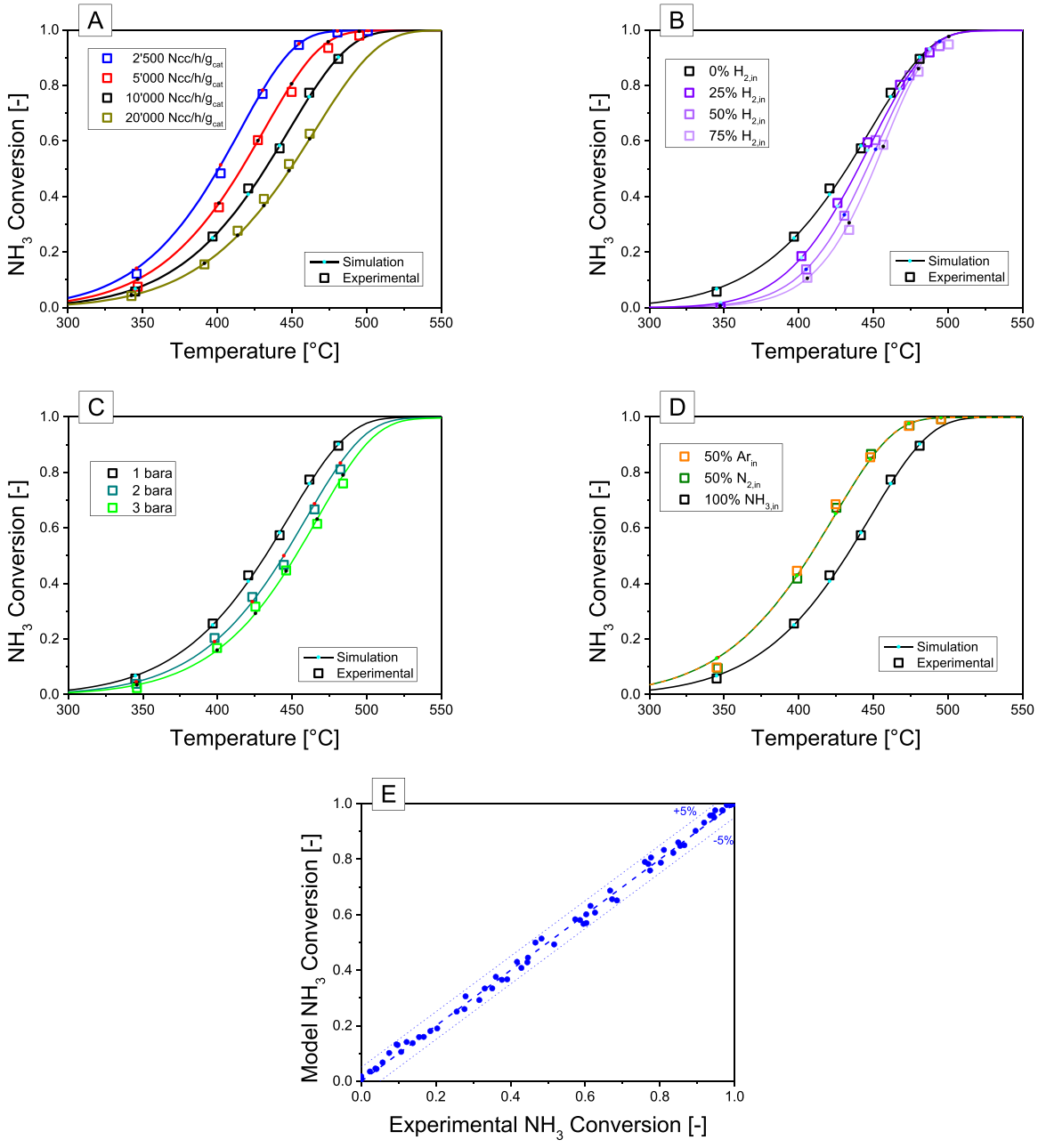

Fig. 11. Experimental versus simulated NH_3 conversion data -3 parameter simplified LHHW Rate Law, Eq. (8).

Industrial cracking units are expected to operate at moderate pressure with a feed of pure ammonia; thus, an engineering relevant reaction rate should be derived in analogous conditions. Furthermore, while many studies of the ammonia decomposition reactions have been performed, no consensus on the actual kinetics has been reached; for this reason, a best fit kinetic expression should be derived in conditions as close as possible to the ones of interest. The main challenge in this context was to design a reactor configuration suitable to carry out experimental runs with pure ammonia while operating in isothermal conditions. In fact, due to the high endothermicity of the reaction ($\Delta H°r = 45.9$ kJ/mol_{NH3}) heat transfer in the reactor becomes a limiting factor that can lead to significant thermal gradients in the catalyst bed, thus, biasing the assessment of the intrinsic reaction rate. The inclusion of a heat conducting continuous aluminium POCS packed with catalyst spherical particles proved to be effective in controlling the temperature gradients. Despite the significant heat demand due to the conversion of a pure ammonia feed, temperature gradients in the catalyst bed were effectively controlled and limited to less than 15 °C. In contrast, an equivalent packed bed reactor, tested in the same reactor/oven configuration and in the same reactive conditions, resulted in temperature gradients in excess of 30 °C. Thanks to the excellent control of the temperature gradients in the reactor, a systematic experimental campaign was carried out on a commercial Ru-Al_2O_3 catalyst, testing the effects of reactants/products concentrations (H_2, N_2, NH_3), temperature (310–550 °C), pressure (1–3 bar-a) and space velocity (2500–20'000 Ncc/h/g_{cat}). Results showed a strong inhibiting effect of H_2 and an overall kinetic order less than 1.

Assuming an ideal isothermal PFR model of the test reactor, conversion data were fitted satisfactorily with a 4-parameter (activation energy, pre-exponential factor and ammonia/hydrogen exponent) power law rate expression; however, a more detailed kinetic analysis was needed to accurately predict the industrially relevant region of high NH_3 conversions. By using the LHHW formalism, several rate expressions derived from different assumptions of RDS and MASI were tested. By taking into account the experimental results as well as the NH_3 and H_2 partial pressure exponents suggested by the power law regression, it was possible to rule out the adsorption/recombinative desorption of the gaseous species as the RDS; however, it was not possible to conclusively ascribe the actual RDS to the second or to the third dehydrogenation step of the mechanism. Nevertheless, the best model (RDS = second dehydrogenation step) provided an excellent fit of all the experimental data, covering a NH_3 conversion range from 1.5 % to 99.7 %. with an average percentage error less than 6 %.

CRediT authorship contribution statement

Federico Sascha Franchi: Writing – original draft, Formal analysis, Data curation, Investigation. **Matteo Ambrosetti:** Writing – review & editing, Investigation, Conceptualization. **Nicola Usberti:** Writing – review & editing, Visualization, Formal analysis. **Alessandra Beretta:** Writing – review & editing, Supervision, Methodology, Conceptualization. **Gianpiero Groppi:** Writing – review & editing, Validation, Methodology, Conceptualization. **Enrico Tronconi:** Writing – review & editing, Supervision, Project administration, Funding acquisition.

Declaration of Competing Interest

The authors declare the following financial interests/personal relationships which may be considered as potential competing interests: Enrico Tronconi reports financial support was provided by European Research Council. Enrico Tronconi is co-editor of the present Special Issue of Applied Catalysis A in honor of Professor's Luca Lietti's 65th birthday. Given his role, he had no involvement in the peer review of this article and had no access to information regarding its peer review. Full responsibility for the editorial process for this article was delegated to another journal editor. If there are other authors, they declare that they have no known competing financial interests or personal relationships that could have appeared to influence the work reported in this paper.

Acknowledgment

We would like to acknowledge the following M.Sc. students at Politecnico di Milano: Veronika Milone and Laura Reggiani, for contributing to the experimental and computational work herein presented, and Ivan Conti, for performing the Ru dispersion measurements.

This project has received funding from the European Research Council (ERC) under the European Union's Horizon 2020 research and innovation program (GA no. 101123385 - INCANT).

Dedication

This paper is dedicated to Professor Luca Lietti on the occasion of his 65th birthday.

Appendix A. Supporting information

Supplementary data associated with this article can be found in the online version at doi:10.1016/j.apcata.2025.120664.

Data availability

Data will be made available on request.

References

[1] L.D.D. Harvey, Global Warming, Routledge, London, 2015, 10.4324/9781315838779.
[2] R. York, S.E. Bell, Energy transitions or additions? Why a transition from fossil fuels requires more than the growth of renewable energy, Energy Res. Soc. Sci. 51 (2019) 40–43, https://doi.org/10.1016/j.erss.2019.01.008.
[3] U.S. Department of Commerce, National Oceanic and Atmospheric Administration, Earth System Research Laboratory, Global Monitoring Division. NOAA report. ⟨http://www.esrl.noaa.gov/gmd/ccgg/trends/index.html⟩.
[4] J.O.M. Bockris, The hydrogen economy: its history, Int. J. Hydrog. Energy 6 (2013) 2579–2588, https://doi.org/10.1016/j.ijhydene.2012.12.026.
[5] J.O. Abe, A.P.I. Popoola, E. Ajenifuja, O.M. Popoola, Hydrogen energy, economy and storage: review and recommendation, Int. J. Hydrog. Energy (29) (2019) 15072–15086, https://doi.org/10.1016/j.ijhydene.2019.04.068.
[6] U.S. Geological Survey, Mineral Commodity Summaries, 2023.
[7] R. Lan, J.T.S. Irvine, S. Tao, Ammonia and related chemicals as potential indirect hydrogen storage materials, Int. J. Hydrog. Energy 37 (2) (2012) 1482–1494.
[8] J.W. Makepeace, T.J. Wood, H.M.A. Hunter, M.O. Jones, W.I.F. David, Ammonia decomposition catalysis using non-stoichiometric lithium imide, Chem. Sci. 6 (7) (2015) 3805–3815.
[9] S. Armenise, E. García-Bordejé, J.L. Valverde, E. Romeo, A. Monzón, A Langmuir–Hinshelwood approach to the kinetic modelling of catalytic ammonia decomposition in an integral reactor, Phys. Chem. Chem. Phys. (2025), https://doi.org/10.1039/C3CP50715G.
[10] C.H. Kunsman, The thermal decomposition of ammonia on iron catalysts. II, J. Am. Chem. Soc. (3) (1929) 688–695, https://doi.org/10.1021/ja01378a005.
[11] J. Ganley, F. Thomas, E. Seebauer, et al., A priori catalytic activity correlations: the difficult case of hydrogen production from ammonia, Catal. Lett. 96 (2004) 117–122, https://doi.org/10.1023/B:CATL.0000030108.50691.d4.
[12] I. Lucentini, X. Garcia, X. Vendrell, Jordi Llorca, Review of the decomposition of ammonia to generate hydrogen, Ind. Eng. Chem. Res. 60 (2021) 18560–18611, https://doi.org/10.1021/acs.iecr.1c00843.
[13] Y. Qui, F.S. Franchi, N. Usberti, A. Beretta, Kinetic investigation of NH3 decomposition over Ru-based catalysts: the limiting role of H* surface coverage and its impact on reactor engineering, Fuel Process. Technol. 276 (2025) 108270, https://doi.org/10.1016/j.fuproc.2025.108270.
[14] S. Sayas, N. Morlanés, S.P. Katikaneni, A. Harale, B. Solami, J. Gascon, High pressure ammonia decomposition on Ru-K/CaO catalysts, Catal. Sci. Technol. (15) (2020) 5027–5035, https://doi.org/10.1039/d0cy00686f.
[15] S.R. Kulkarni, N. Realpe, A. Yerrayya, V.K. Velisoju, S. Sayas, N. Morlanes, J. Cerillo, S.P. Katikaneni, S.N. Paglieri, B. Solami, J. Gascon, P. Castaño, Elucidating the rate-determining step of ammonia decomposition on Ru-based catalysts using ab initio-grounded microkinetic modelling, Catal. Sci. Technol. (7) (2023) 2026–2037, https://doi.org/10.1039/D3CY00055A.
[16] I. Lucentini, G.G. Colli, C.D. Luzi, I. Serrano, O.M. Martínez, J. Llorca, Catalytic ammonia decomposition over Ni-Ru supported on CeO2 for hydrogen production, Appl. Catal. B 286 (2021) 119896, https://doi.org/10.1016/j.apcatb.2021.119896.

[17] V. Prasad, A.M. Karim, A. Arya, D.G. Vlachos, Assessment of overall rate expressions and multiscale, microkinetic model uniqueness via experimental data injection: ammonia decomposition on Ru/γ-Al2O3 for hydrogen production, Ind. Eng. Chem. Res. 48 (2009) 5255–5265, https://doi.org/10.1021/ie900144x.
[18] R. Balzarotti, M. Ambrosetti, A. Beretta, G. Groppi, E. Tronconi, Investigation of packed conductive foams as a novel reactor configuration for methane steam reforming, Chem. Eng. J. 391 (2020) 123494, https://doi.org/10.1016/j.cej.2019.123494.
[19] F. Zaio, M. Ambrosetti, C. Tregambe, A. Beretta, G. Groppi, E. Tronconi, Intensification of methane steam reforming by Cu-foams packed with Rh-Al2O3 catalyst: a pilot-scale assessment, Chem. Eng. Res. Des. 215 (2025) 98–107, https://doi.org/10.1016/j.cherd.2025.01.022.
[20] L. Fratalocchi, G. Groppi, C.G. Visconti, L. Lietti, E. Tronconi, Adoption of 3D printed highly conductive periodic open cellular structures as an effective solution to enhance the heat transfer performances of compact Fischer-Tropsch fixed-bed reactors, Chem. Eng. J. 386 (2020) 123988, https://doi.org/10.1016/j.cej.2019.123988.
[21] M. Bracconi, M. Ambrosetti, M. Maestri, G. Groppi, E. Tronconi, Analysis of the effective thermal conductivity of isotropic and anisotropic periodic open cellular structures for the intensification of catalytic processes, Chem. Eng. Process.: Process Intensif. 158 (2020) 108169, https://doi.org/10.1016/j.cep.2020.108169.
[22] M. Ambrosetti, G. Groppi, W. Schwieger, E. Tronconi, H. Freund, Packed periodic open cellular structures – an option for the intensification of non-adiabatic catalytic processes, Chem. Eng. Process.: Process Intensif. 155 (2020) 108057, https://doi.org/10.1016/j.cep.2020.108057.
[23] M. Panzeri, C.G. Visconti, G. Groppi, E. Tronconi, Process intensification of the Fischer-Tropsch synthesis using conductive packed POCS with skin: the role of the POCS design parameters, Chem. Eng. J. 521 (2025) 123359, https://doi.org/10.1016/j.cej.2025.166359.
[24] L. Fratalocchi, G. Groppi, C.G. Visconti, L. Lietti, E. Tronconi, Packed-POCS with skin: a novel concept for the intensification of non-adiabatic catalytic processes demonstrated in the case of the Fischer-Tropsch synthesis, Catal. Today 383 (2022) 15–20, https://doi.org/10.1016/j.cattod.2020.12.031.
[25] Metals Handbook, 10th ed., vol. 1, ASM International Handbook Committee, ASM International, Materials Park, OH, 1990.
[26] C.G. Visconti, E. Tronconi, L. Lietti, P. Forzatti, S. Rossini, R. Zennaro, Detailed kinetics of the Fischer-Tropsch synthesis on cobalt catalysts based on H-assisted CO activation, Top. Catal. 54 (2011) 786–800, https://doi.org/10.1007/s11244-011-9700-3.
[27] A.C. Hindmarsh, Large ordinary differential equation systems and software1, IEEE Control Syst. Mag. 2 (1982) 24–30, https://doi.org/10.1109/MCS.1982.1103756.
[28] V. Specchia, G. Baldi, S. Sicardi, Heat transfer in packed bed reactors with one phase flow, Chem. Eng. Commun. 4 (1980) 361–380, https://doi.org/10.1080/00986448008935916.
[29] J.C. Ganley, F.S. Thomas, E.G. Seebauer, R.I. Masel, A priori catalytic activity correlations: the difficult case of hydrogen production from ammonia, Catal. Lett. 96 (2004) 117–122, https://doi.org/10.1023/B:CATL.0000030108.50691.d4.
[30] K. Lamb, S.S. Hla, M. Dolan, Ammonia decomposition kinetics over LiOH-promoted, A-Al2O3-supported Ru catalyst, Int. J. Hydrog. Energy 44 (2019) 3726–3736, https://doi.org/10.1016/j.ijhydene.2018.12.123.
[31] K.E. Lamb, D.M. Viano, M.J. Langley, S.S. Hla, M.D. Dolan, High-purity H2 produced from NH3 via a ruthenium-based decomposition catalyst and vanadium-based membrane, Ind. Eng. Chem. Res. (23) (2018) 7811–7816, https://doi.org/10.1021/acs.iecr.8b01476.
[32] L.J. Gillespie, J.A. Beattie, The thermodynamic treatment of chemical equilibria in systems composed of real gases. I. An approximate equation for the mass action function applied to the existing data on the haber equilibrium, Phys. Rev. 36 (1930) 743, https://doi.org/10.1103/PhysRev.36.743.
[33] G. Buzzi Ferraris, G. Donati, F. Rejna, S. Carrà, An investigation on kinetic models for ammonia synthesis, Chem. Eng. Sci. 29 (1974) 1621–1627, https://doi.org/10.1016/0009-2509(74)87013-2.